Two-photon photostimulation and imaging of neural circuits

Volodymyr Nikolenko, Kira E Poskanzer & Rafael Yuste

We introduce an optical method to stimulate individual neurons in brain slices in any arbitrary spatiotemporal pattern, using two-photon uncaging of MNI-glutamate with beam multiplexing. This method has single-cell and three-dimensional precision. By sequentially stimulating up to a thousand potential presynaptic neurons, we generated detailed functional maps of inputs to a cell. We combined this approach with two-photon calcium imaging in an all-optical method to image and manipulate circuit activity.

Neuronal circuits are composed of many cell types, and it is likely that each cell type carries out a specialized function[1]. Therefore, as a prerequisite to understanding the function of a circuit, it appears necessary to map synaptic connections among different types of neurons or to map all connections made onto a given cell[2].

After early work using fluorescent membrane probes[3], photostimulation of neurons using caged glutamate[4] has greatly advanced this research program, generating high-resolution input maps of neurons in brain slices[4–10]. In this method, glutamate is uncaged by focusing ultraviolet light at a particular position in the brain slice and simultaneously recording intracellular responses from a neuron at a different location. By moving the uncaging beam systematically across the brain slice, one can map the territories that generate excitatory or inhibitory responses in the recorded cell. Although very useful, this method suffers from the problem that, because of the inherent scattering of light in living tissue and the large uncaging area generated by one-photon excitation, the stimulated area contains more than one neuron. Thus, one-photon photostimulation has not revealed synaptic connections between cells, but instead connections between a particular territory and a recorded neuron.

To stimulate individual cells, we took advantage of the exquisite spatial resolution of two-photon excitation[11]. We developed a two-photon photostimulation method, wherein a beam-multiplexed two-photon laser is moved from neuron to neuron to uncage glutamate and sequentially make each neuron fire, while the resulting synaptic potential in a particular cell is simultaneously recorded. This allows for the detection of monosynaptically connected cells and for input maps to be built with single-cell resolution. We combined this method with two-photon calcium imaging to manipulate and simultaneously record circuit activity.

RESULTS

Optical design and labeling of neurons

We developed a method to photostimulate and image the activity of large neuronal populations using a single laser (**Fig. 1** and **Supplementary Fig. 1** online). Custom software allowed us to position of the laser beam in any arbitrary point in the field of view and to quickly switch between two-photon calcium imaging of indo-1 acetoxymethyl (AM) ester (indo-1 AM) and two-photon uncaging of 4-methoxy-7-nitroindolinyl (MNI)-caged L-glutamate[12,13] on individual neurons, causing them to fire action potentials. We used an electro-optical modulator for switching between two laser light intensities: a lower intensity for imaging and a higher intensity for uncaging. Thus, we used the same laser beam (at 725 nm) to trigger and monitor circuit activity.

To visualize cell bodies of neurons and detect their coordinates, we loaded acute neocortical slices from mouse somatosensory and visual cortex with membrane-permeant AM-ester calcium indicators. Because 700–735 nm light is required for two-photon uncaging of MNI-caged L-glutamate, we chose indo-1 AM as the calcium indicator. Indo-1 AM produced good loading of neurons[14] and excellent calcium sensitivity in response to action potentials (**Fig. 1**). In addition, the low-affinity calcium indicator mag-indo-1 AM loaded neocortical slices more efficiently than indo-1 AM. Even though mag-indo-1 AM is not suitable for optical monitoring of action potentials (due to its low affinity for calcium), it proved very useful for fluorescent labeling of neuronal somata (**Supplementary Fig. 2** online) for experiments that did not require calcium imaging (for example, in input mapping experiments). For combined imaging/uncaging experiments, it was possible to jointly label with both indicators to obtain robust labeling of the neurons by mag-indo-1 AM, while still benefiting from the functional calcium sensitivity of indo-1 AM.

Indo-1 AM and mag-indo-1 AM loaded most neurons but not glia, as determined by dual labeling with sulforhodamine 101 (ref. 15; **Supplementary Fig. 3** online). Only 5.7 ± 1.56% of mag-indo-1 AM–loaded cells were also loaded with sulforhodamine 101,

Howard Hughes Medical Institute, Department of Biological Sciences, Columbia University, 1212 Amsterdam Avenue, Box 2435, New York, New York 10027, USA. Correspondence should be addressed to V.N. (vn59@columbia.edu).

RECEIVED 3 MAY; ACCEPTED 23 SEPTEMBER; PUBLISHED ONLINE 28 OCTOBER 2007; DOI:10.1038/NMETH1105

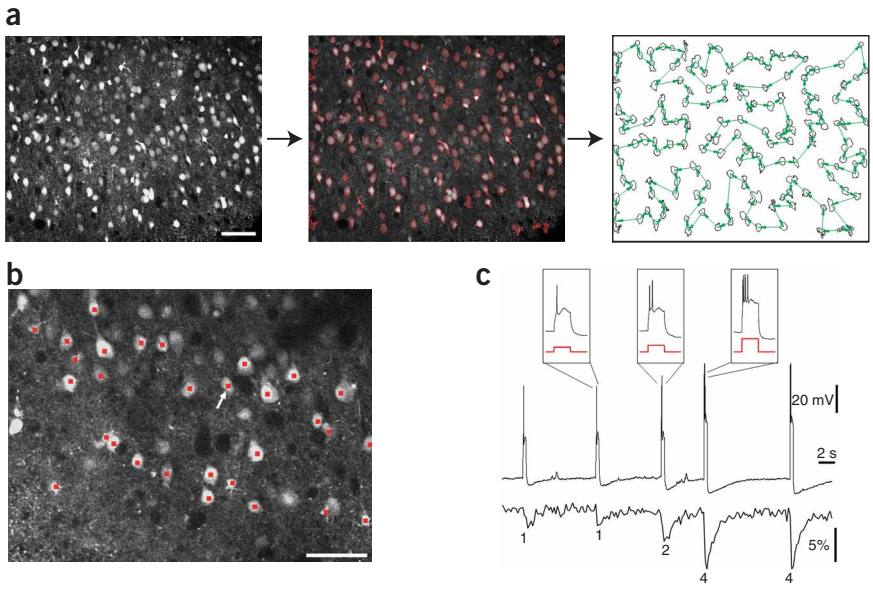

Figure 1 | Targeted imaging of neuronal populations. (**a**) The original two-photon image (left) was analyzed online, cell contours were automatically detected (middle) and a convex-hull traveling-salesman algorithm computed the shortest scanning path between all cells (right). Micrograph, a P13 neocortical slice loaded with indo-1 AM, and imaged with 730-nm excitation and a 40×, 0.8 NA objective. (**b**) For calcium imaging of targeted neurons, a P14 neocortical slice was loaded with indo-1 AM and a group of neurons (red) was selected for vector-mode imaging. A patch-clamped cell (arrow) was filled with 50 μM indo-1-K. Note that fluorescence intensity is similar in loaded and patch-clamped cells. Image taken at 735-nm excitation, with a 40×, 0.8 NA objective. Scale bars, 50 μm. (**c**) To assess single action potential sensitivity of calcium imaging, action potentials (voltage recordings in black; holding potential, −65 mV) were induced by injection of current pulses (red traces in insets). The corresponding calcium signals (lower trace; relative change in fluorescence $\Delta F/F$) from the patched neuron showed clear responses to one or more spikes (number of action potentials indicated below optical traces).

and only 8.1 ± 2.59% ($n = 4$ slices) of sulforhodamine 101–loaded cells were also loaded with mag-indo-1 AM.

Cell detection, fast scanning and action-potential imaging

Once brain slices were loaded and an image was acquired, we detected the position of 500–4,000 neurons automatically. We used an algorithm[16] to detect the center of mass coordinates of all visible neurons from two-photon fluorescence images (**Fig. 1a**). Then, with custom-designed software[17] we implemented a special scanning regime, which we call 'vector mode', to perform simultaneous imaging and photoactivation. In contrast to raster scanning, in vector mode the laser sequentially visits a user-selected set of points of interest ('targets', which are in this case neuronal cell bodies) to perform point-measurements of fluorescence and/or photoactivate light-sensitive compounds, at a predefined duration and laser intensity. To optimize the scanning pattern, reduce delays between scanning points and minimize the wear of galvanometer scan mirrors, we reordered the sequence of targets using a fast algorithm that finds a near-optimal solution to the traveling salesman problem (**Fig. 1a**; 'convex-hull' algorithm).

We next tested whether vector-mode scanning could detect the calcium signals generated by action potentials, induced by injection of current. For these experiments, we filled neurons with 50 μM indo-1 pentapotassium salt (indo-1-K) via a patch-clamp pipette. This intracellular concentration approximately corresponds to the intracellular concentration of the indicator obtained by AM-dye loading[18] (**Fig. 1b**). Under these conditions, we reliably measured calcium signals caused by individual action potentials with good signal-to-noise ratio (5 ms laser exposure per cell; **Fig. 1c**).

Multiplexed laser uncaging

We then developed an optical method to reliably elicit action potentials in neurons by uncaging glutamate. In our experience, the point spread function of two-photon excitation is too small to release enough free glutamate to effectively depolarize a neuron to action potential threshold (**Supplementary Note** online). To make neurons fire action potentials reliably, we therefore placed several uncaging locations over the soma of the targeted cell, by multiplexing the uncaging in time or in space (**Fig. 2**). We achieved temporal multiplexing (that is, sequential uncaging) by positioning the laser sequentially in a circular pattern of positions (**Fig. 2a**). These 'complex' stimulation targets[10] had a diameter similar to that of the stimulated neuron, and the spatial resolution of their uncaging response was also comparable to the average diameter of a cell body (**Fig. 2b**). For simultaneous imaging and uncaging experiments, we positioned a single imaging target (**Fig. 2a**,**c**) in the center of the stimulation targets with a vector-mode scan at lower laser power.

To shorten the time necessary for cells to reach action potential threshold and more effectively use the available laser power, we also used spatial multiplexing, splitting the laser beam into several closely spaced beamlets for simultaneous uncaging of several different locations around the cell somata (**Fig. 2c**). We used a diffractive optical element (DOE)[19], an efficient single-element beam-splitter suitable for nonlinear microscopy, placed at the plane optically conjugated to the scanning mirrors (**Supplementary Fig. 1**). The DOE we selected produces a symmetrical linear 5-spot pattern in the far field (first diffraction order; **Fig. 2d**) that generated a beamlet pattern approximately the size of a neuronal soma (**Fig. 2c**).

The combination of temporal and spatial beam multiplexing allowed us to use shorter uncaging pulses. Most neurons were easily stimulated to fire a short burst of ~3–7 action potentials with 10–13 ms uncaging pulses, although it was possible to induce individual action potentials with pulses as short as 5 ms (**Fig. 2e**). The DOE not only increased the efficiency of uncaging but also improved the imaging signal-to-noise ratio because the photomultiplier sampled five spatially different somatic locations illuminated simultaneously by separate beamlets.

We measured the axial resolution of these beam-multiplexed uncaging methods by monitoring both the two-photon fluorescence and the action potential responses of a neuron, while systematically changing the focal plane of the uncaging laser. In these experiments, an axial displacement of ~30 μm effectively

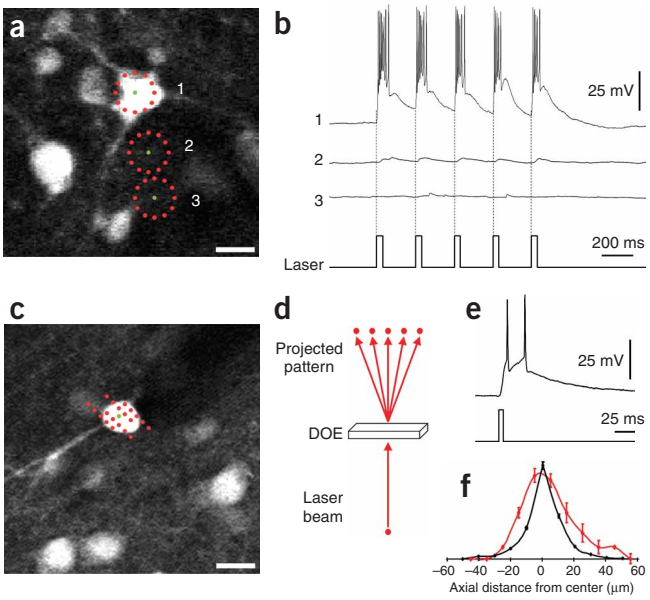

Figure 2 | Two-photon photostimulation with beam multiplexing. (**a**) Image of a patched cell and location of three sets of 12 uncaging targets forming a circle (red dots), which were sequentially stimulated (2.5 ms/point). Green dot is the imaging target (5 ms). (**b**) Electrophysiological recordings of the neuron during uncaging at positions shown in **a** (top). Note how uncaging in position 1 triggers a burst of action potentials (holding potential –65 mV; bottom trace, laser pulse). In positions 2 or 3, the action potential threshold is not reached. (**c**) Neuron stimulated by a linear DOE pattern (red dots, uncaging targets; green dot, imaging target). (**d**) The DOE splits the beam spatially, illuminating 5 spots simultaneously, thus shortening the uncaging time required to reach action potential threshold. DOE and sequential uncaging are combined in **c**, so a total of 20 spots are illuminated, five at a time. (**e**) Example of DOE photostimulation, illustrating the briefer uncaging time to generate spiking (plots as in **b**). (**f**) Depth resolution of beam multiplexing two-photon uncaging. Red curve is number of action potentials induced by uncaging pulses at different depths, normalized to maximum number of action potentials induced. Black curve is two-photon fluorescence of each focal plane, normalized to the maximum fluorescence of the soma. Notice the close correspondence between these two curves. Thus, the axial resolution of two-photon photostimulation closely follows the three-dimensional sectioning properties of two-photon fluorescence imaging. Uncaging performed with 4 × 3 ms, 5-beamlet DOE protocol with a 20×, 0.5 NA objective. Error bars, s.e.m. Scale bars, 10 μm.

prevented the response of the neuron to the uncaging pulse (**Fig. 2f**). As expected, the two-photon fluorescence profile was also dependent on the focal plane (**Fig. 2f**). These results demonstrate the optical sectioning capabilities of our uncaging method.

Two-photon mapping of monosynaptic inputs

We next mapped the synaptic inputs to different neurons by performing current-clamp recordings on selected neurons while sequentially photostimulating most, or all, AM dye–labeled neurons in the surrounding area of a brain slice (**Fig. 3**, $n = 169$ maps; **Supplementary Methods** online). In a typical experiment with a 10× objective our algorithm detected about 700–5,000 loaded cells in a single focal plane of a brain slice, encompassing all six cortical layers (**Supplementary Fig. 2**). Although we stimulated every single detected cell in some experiments, to complete the protocol in a reasonable time we often restricted the number of neurons stimulated to 500 by targeting neurons in a pseudorandom fashion (**Supplementary Methods**). As a control, we also stimulated patched cells by uncaging at the end of the photostimulation protocol.

In these mapping experiments, we encountered two distinct classes of postsynaptic responses time-locked to the uncaging pulses (**Fig. 3a**,**b** and **Table 1**). These events closely resembled the two types of events described during one-photon glutamate uncaging[7]: compound monosynaptic excitatory postsynaptic potentials (EPSPs) induced by short bursts of action potentials in presynaptic photostimulated cells ('true positives'; **Fig. 3a**) and larger, slower depolarizations with shorter latencies, presumably caused by direct uncaging onto distal dendrites of the patch-clamped cells ('false positives'; **Fig. 3b**). Although dendrites were not visible with our loading conditions, and only cell bodies were targeted by the stimulation protocol, it is still conceivable that dendrites could cross near a stimulated area and thus be stimulated directly. It was possible to distinguish between true and false positives based on their statistically different onset kinetics and latencies to the uncaging pulse (**Table 1**). Moreover, as one might expect, the false positive signals traced the dendritic tree of the postsynaptic cell (**Fig. 3b**), whereas the true positive signals did not (**Fig. 3a**).

We confirmed the sorting of true and false positive responses by applying the sodium channel blocker tetrodotoxin (1 μM) to block action-potential generation in the brain slice. This prevents all evoked synaptic release, revealing solely false positive responses. By comparing these results with those obtained in the absence of tetrodotoxin, we found that the probability to incorrectly score false positives as true positives was small (0.45% on average, $n = 17$ maps). In contrast, our sorting criteria based on kinetics classified more signals as false positives than were found using tetrodotoxin. Specifically, whereas 99.3% of tetrodotoxin false positives were also identified as such previously, only 84% of labeled false positives were confirmed as such by mapping in the presence of tetrodotoxin.

Finally, using dual whole-cell recordings, we found that neurons that generated true positive signals after being stimulated by the uncaging were indeed monosynaptically connected to the patch-clamped postsynaptic neuron (**Fig. 3c–f**). Action potentials elicited in putative presynaptic neurons reliably triggered excitatory postsynaptic responses in the postsynaptic cell with short delays, corresponding to monosynaptic connections (**Fig. 3d–f**; average delay was 1.83 ± 0.50 ms, ranging from 0.79 to 3.49 ms; $n = 5$ connected pairs).

Functional maps of synaptic properties

Our method allowed us to identify putative presynaptic neurons, measure their synaptic properties (such as amplitude, onset and offset kinetics of unitary synaptic EPSPs) and build maps of their spatial distribution (for amplitude maps see **Fig. 3a** and **Supplementary Fig. 4** online). Because uncaging generated short bursts of action potentials in the stimulated cells, it was also possible to measure, for each input cell, more complex synaptic properties such as rate of facilitation or depression, total amplitude of compound EPSP, accommodation after several photostimulation pulses and other variables (data not shown).

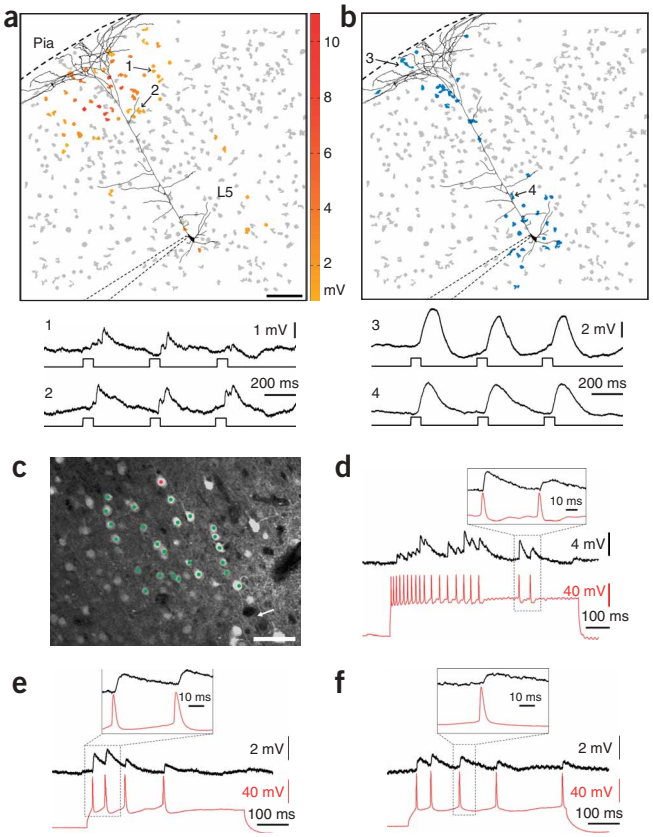

Figure 3 | Mapping inputs with single cell resolution. (**a**) Input map for a layer 5 pyramidal neuron and super-imposed morphological reconstruction of its dendritic tree (top). Gray areas outline stimulated neurons. Colored areas are outlines of all 'true positive' cells, color-coded according to peak EPSP amplitude. Dotted outline marks the patch pipette location. Scale bar, 100 μm. Voltage recordings (upper traces) from the patched cell during uncaging (laser pulses in lower traces) in locations labeled by arrows in **a** (bottom). Holding potential, −65 mV. Pia, pial surface. (**b**) False positive map for the same neuron (blue areas; top). Note that it tracks the morphology of the dendritic tree. Recordings of false positive signals during uncaging in locations labeled by arrows (bottom). Note the difference in kinetics and amplitude between true and false positive signals. (**c**) True positive signals are monosynaptic connections. A post-synaptic neuron was patched (not in focus; arrow) and all neurons labeled by green dots were sequentially stimulated. The neuron labeled by a red dot gave a true positive signal and was subsequently patch-clamped. Note the distance between both neurons. Scale bar, 50 μm. (**d**) Dual recording from these two neurons reveals monosynaptic connection. Action potentials induced by current injection in the putative presynaptic neuron (red; neuron labeled by the red dot in **c**) cause time-locked EPSPs in the postsynaptic cell (black). Inset: note correspondence between onset of action potentials and EPSPs. Both neurons were held at −63 mV. (**e**,**f**) Examples of monosynaptically connected true positive cells from two other experiments.

Input maps in three dimensions

To demonstrate the optical sectioning capabilities of the uncaging and the accuracy of our input maps, we performed mapping in two different focal planes separated by 45 μm (**Fig. 4**). This separation was required to ensure that neurons in neighboring focal planes were not stimulated (**Fig. 2f**), and, indeed, we obtained negligible overlap between connectivity maps obtained in these two different focal planes. Specifically, only 2 out of 300 target coordinates selected at one focal plane yielded true positive responses in both focal planes, confirming the optical sectioning ability of our two-photon uncaging protocol. Thus, independent inputs maps can be built with a depth resolution that is sufficient to resolve an average-sized neuronal cell body.

Input maps from adjacent cells

We routinely recorded from several neurons simultaneously to improve the efficiency of our mapping experiments (**Supplementary Fig. 4**). In all, we recorded 26 single cell maps, 16 simultaneous maps of pairs of neurons, 25 of triplets and 9 of quadruplets, for a total of 169 maps. Although the analysis of the spatial properties of these maps is beyond the scope of this manuscript, an interesting preliminary result was that even very closely positioned layer-5 pyramidal cells could have very different input maps (**Supplementary Fig. 4**), consistent with the possibility that functional independent networks of cortical neurons are superimposed in the same cortical territories[20].

Repeatability of input maps

We verified the stability of the input maps, and the repeatability of the stimulation protocol and analysis by using a shortened version of the protocol, with ~5–8-min intervals between trials ($n = 7$ postsynaptic neurons; **Fig. 5**). These maps revealed remarkable repeatability, and the shapes of EPSPs from selected cells were also similar from trial to trial (**Fig. 5**). Specifically, 77.1 ± 12% of all true positive cells were scored as such in every trial (mean ± s.d.; $n = 7$ cells, >7 trials each). This demonstrates that the protocol can produce reliable maps, and that the uncaging experiment did not compromise the health of stimulated neurons. At the same time, we noticed a small trial-to-trial variability in the input maps (**Fig. 5**), perhaps explained by an inconsistency in the number of action potentials generated by the uncaging pulses. This variability, however, could also reflect spontaneous fluctuation of synaptic weights or synaptic rewiring, as has been recently suggested[21]. These

Table 1 | Analysis of true and false positive responses

	True positives				False positives			
	Amplitude of first EPSP (mV)	Peak amplitude (mV)	Latency after laser pulse (ms)	Rise speed (mV/ms)	Amplitude of first EPSP (mV)	Peak amplitude (mV)	Latency after laser pulse (ms)	Rise speed (mV/ms)
Mean	1.04	3.21	57.85	0.066	5.69	5.76	30.00	0.056
Standard deviation	0.26	1.16	6.46	0.021	2.00	1.83	9.35	0.016
Standard error	0.11	0.52	2.89	0.009	0.89	0.82	4.18	0.007
P value (two tail)	1.77×10^{-13}	2.84×10^{-5}	9.89×10^{-20}	0.0365				

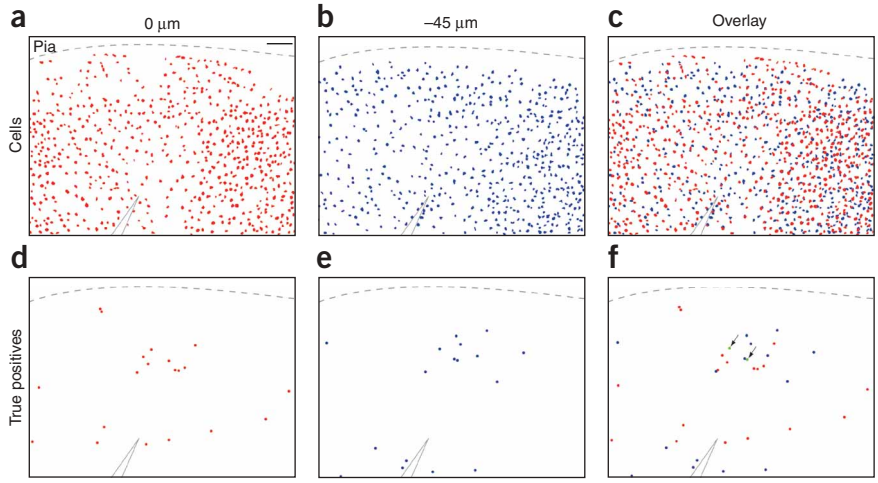

Figure 4 | Mapping inputs in three dimensions. (**a**) Map of all mag-indo-1 AM–loaded cells ($n = 635$) detected at a superficial focal plane of the slice (0 µm). We stimulated 300 positions out of these 635 to test for potential connectivity. Gray outline marks the patch pipette location. Pia, pial surface. Scale bar, 100 µm. (**b**) Map of loaded cells ($n = 546$) 45 µm below those mapped in **a**. The difference between cell positions at those two focal planes is shown by the overlay in **c**. (**d**) Positions ($n = 20$) that produced true positive responses in the patched cell while stimulated at focal plane in **a**. (**e**) Positions ($n = 17$) that generated true positive responses at focal plane in **b**. The 300 coordinates tested were identical to those used in **d**. (**f**) Overlay of inputs maps, which overlap at only two positions (arrows, green dots), demonstrating the ability of selectively mapping inputs at two adjacent focal planes.

possibilities will be examined in future studies. Thus, our method could be used, in principle, to study cortical plasticity in long-term experiments.

Simultaneous two-photon stimulation and imaging

We next combined our photostimulation method with calcium imaging of neuronal populations[22] (**Fig. 6**). We easily detected single spikes with vector-mode calcium imaging when action potentials were induced, either by current injections (**Fig. 1c**) or by two-photon uncaging (**Fig. 6a**). We also detected similar calcium transients in photostimulated cells that were not patched (**Fig. 6a**) as if the uncaging generated action potentials in them.

We then sequentially stimulated every detected neuron (usually up to a hundred)—as when one plays a piano one note at a time—while simultaneously imaging all cells (**Fig. 6b**). In these experiments, we noticed that calcium transients, time-locked to the uncaging pulses, were occasionally present in cells that were not photostimulated (**Fig. 6b**; responses in cell 1 when stimulating cell 2). These unstimulated neurons that exhibited calcium transients

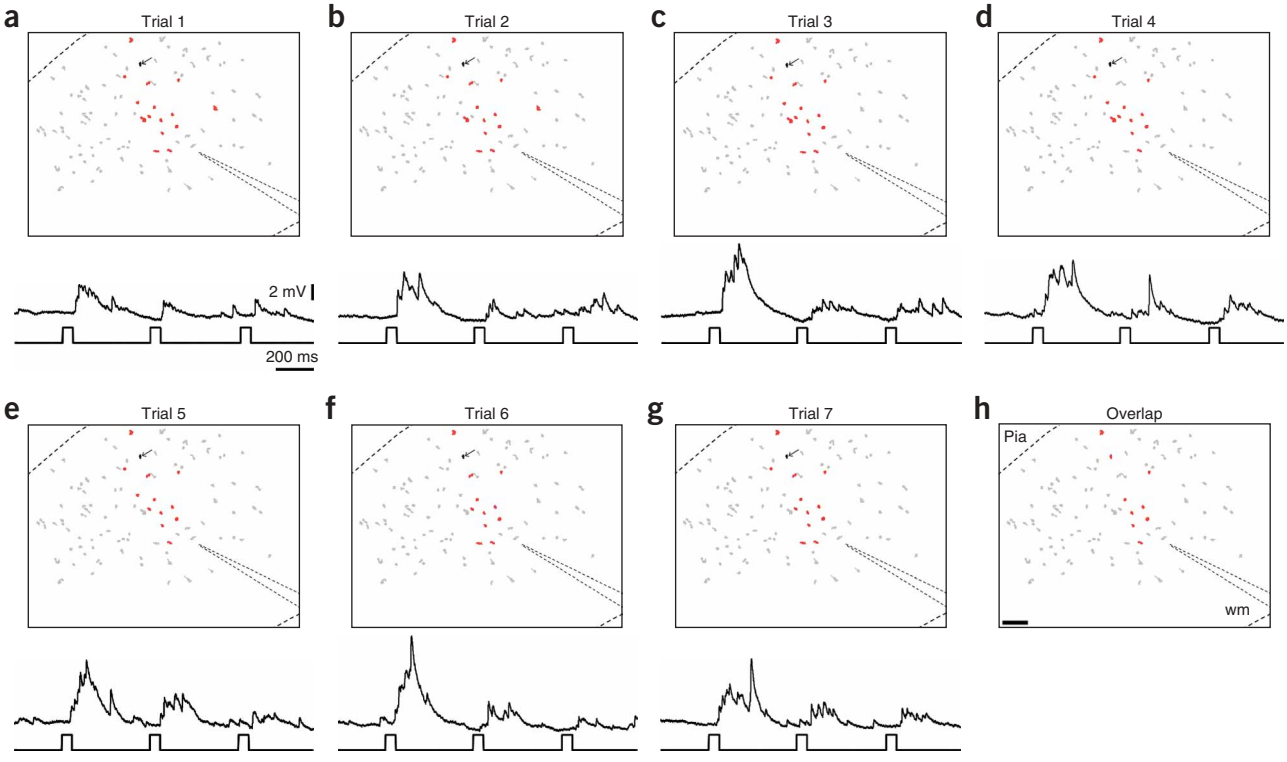

Figure 5 | Reproducibility of input maps. (**a**–**g**) Seven consecutive input maps from the same neuron (marked by tip of pipette outline), obtained sequentially over approximately 1 h (top). Gray areas are stimulated cells, and red areas are cells generating true positive signals. EPSPs (upper traces; holding potential, –65 mV) generated by uncaging (lower traces; laser pulses) the black cell labeled by the arrow (bottom). (**h**) Locations that produced a true positive response in every map. Scale bar, 100 µm.

were often located far from the stimulated cells, implying that the action potentials that triggered the optical signals were not a consequence of direct stimulation of their dendrites. Thus, we attributed these functional signals in distant cells to action potentials induced by strong excitatory connections from photostimulated neurons. Indeed, strongly facilitating monosynaptic connections that can fire a postsynaptic cell have been reported, for example, between pyramidal excitatory cells and low-threshold spiking interneurons[23,24].

Finally, we extended our method to the quasi-simultaneous stimulation of groups of cells (five neurons, 60–90 ms total uncaging time)—as when one plays a piano a chord at a time—while simultaneously imaging all cells (**Fig. 6c**). In eight different experiments, we detected synchronized calcium transients in unstimulated cells, time-locked to the stimulation of particular combinations of other neurons (**Fig. 6c** and **Supplementary Fig. 5** online). These global activations were similar to those observed under some types of epileptiform events in other experiments[25,26].

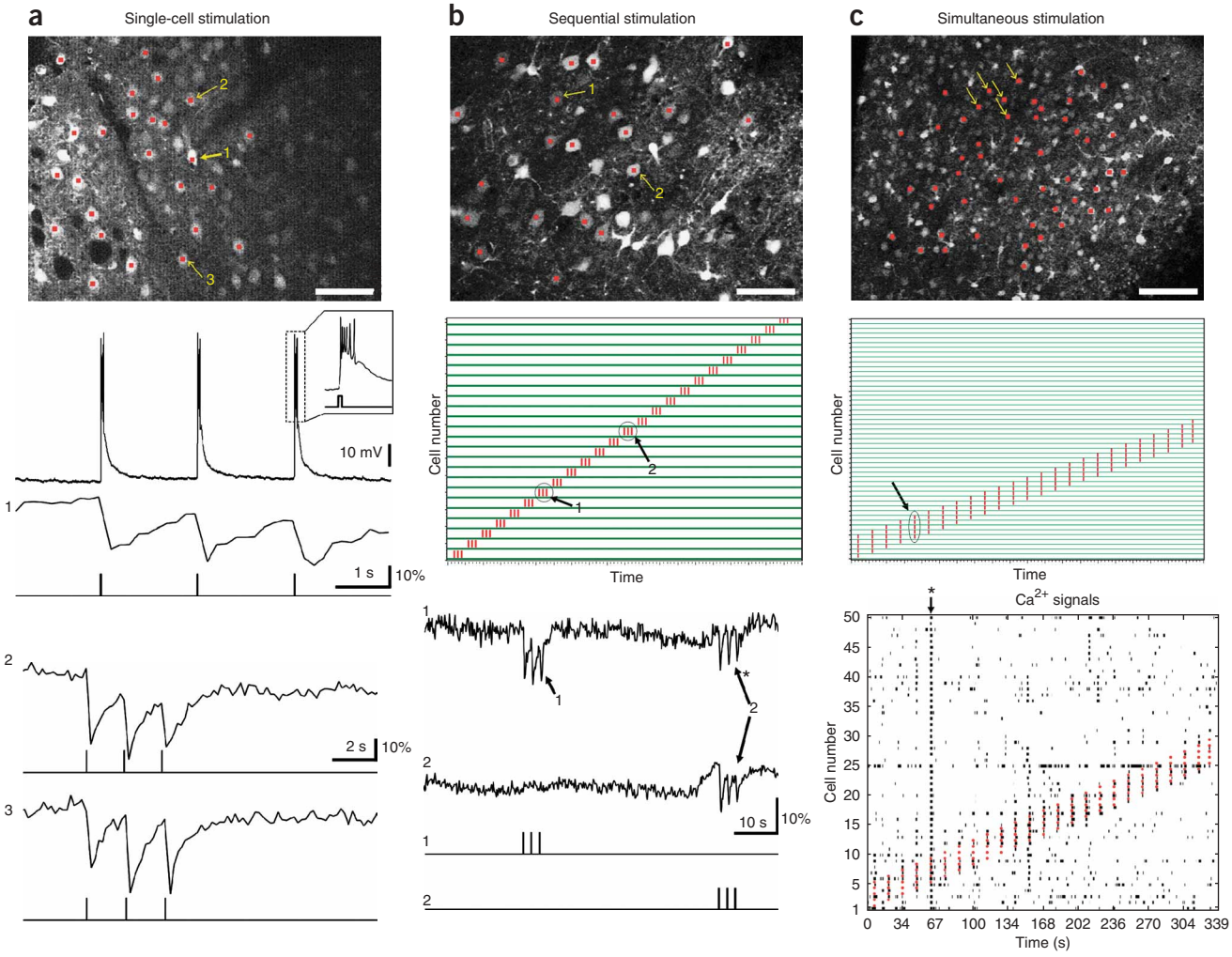

Figure 6 | All-optical stimulation and imaging of network activity. (**a**) Optical detection of uncaging responses in single cells. Neurons labeled by red markers were photostimulated sequentially and simultaneously imaged in vector mode (top). Electrophysiological (upper trace) recordings of neuron 1, and fluorescence calcium measurements from neurons 1, 2 and 3 (middle traces, $\Delta F/F$) during uncaging on their cell bodies (lower trace, laser pulses) (bottom). Note how uncaging triggers action potentials in neuron 1 (inset), loaded with indo-1-K 50 μM through the patch pipette, producing easily detectable calcium signals. Uncaging on neurons 2 and 3 (not patched and loaded by indo-1 AM) generates calcium signals of similar amplitude to those in neuron 1, presumably also owing to action potential activity. Imaging and uncaging performed with complex DOE targets (imaging, 5 ms/neuron; uncaging: 4 × 2.5 ms/neuron). Scale bar, 50 μm. (**b**) Sequential stimulation with simultaneous imaging of multiple cells. Fifty neurons, labeled by red markers, were continually imaged while being sequentially photostimulated (top). Protocol of the experiment, in which every neuron is imaged (green lines) while neurons marked with red vertical bars are being stimulated (middle). Activation of one neuron by the stimulation of another (bottom). Upper traces are fluorescence measurements and bars are laser pulses. Uncaging pulses on neuron 1 generate calcium transients (presumably owing to action potentials) in neuron 1, whereas uncaging over neuron 2 generates calcium transients, not only in this neuron, but also in neuron 1. Joint mag-indo-1 AM and indo-1 AM loading. Scale bar, 50 μm. (**c**) Simultaneous stimulation and imaging. Experiment similar to that shown in **b**, but with different sets of 5 neurons stimulated simultaneously (yellow arrows), while all 50 neurons (red markers) are imaged (top). Protocol of the experiment displays the sequential activation of sets of five neurons (red lines), during the imaging of all other ones (green traces) (middle). For each cell, displayed on *y* axis, black tick marks represent detected calcium transients, and red dots mark stimulated neurons (bottom). Note that synchronous stimulation reliably triggers calcium transients in the stimulated cells but can also generate network activity (vertical arrays of black lines in nonstimulated neurons), in some cases leading to a synchronized activation of most of the imaged cells (star). A higher-resolution image is available in **Supplementary Fig. 5**. Joint indo and mag-indo AM loading. Scale bar, 100 μm.

Consistent with this, we observed paroxysmal depolarization shifts by simultaneous electrophysiological recordings (data not shown). Although we occasionally observed similar epileptiform events spontaneously in brain slices perfused with MNI-glutamate, the fact that they were time-locked to the photostimulation of a specific set of neurons demonstrates that the stimulation of very few neurons can be sufficient to trigger an epileptiform event in the brain slice.

DISCUSSION

We describe the two-photon photostimulation of neuronal circuits at single-cell resolution in combination with calcium imaging. By systematically uncaging glutamate on the somata of hundreds of neurons while recording the intracellular activity of a cell of interest, we obtained single-cell resolution maps of excitatory connections in the brain slice. Using our method, the neurons are detected automatically and the stimulation procedure is under computer control, so it is feasible to sample relatively quickly (<5 min) a large number of neurons (up to 1,000), and test whether or not they are connected to the recorded cell. Using dual whole-cell recordings, we confirmed that putative input cells are monosynaptically connected to the recorded neuron. We therefore interpret the map of true positive inputs as the map of neurons presynaptic to the recorded cell. In addition, these maps can be obtained in three dimensions, so one could, in principle, sample all the cells in the tissue and test whether they are presynaptic to any given cell.

In addition to anatomical mapping, this method can be used to map functional synaptic properties. The number of synaptic contacts could be estimated from the amplitude of the synaptic response, and other properties such as the failures or synaptic dynamics may be obtained by additional analysis. We obtained similar maps to the ones presented in voltage clamp, thus permitting a biophysical analysis of EPSCs from different presynaptic neurons. Furthermore, as several neurons can be patched at the same time, simultaneous functional maps can be obtained and compared (**Supplementary Fig. 4**). Also, because these input maps can be obtained quickly, this technique can be used to monitor changes in synaptic connectivity[21]. Finally, although we exclusively mapped EPSPs here, one can also detect inhibitory postsynaptic potentials, so this technique can be extended to map inhibitory connections and could reveal the matrix of synaptic weights of a neuron, getting closer to the goal of visualizing all the connections onto a given cell[2].

The ability to analyze and visualize input maps online allows for an expansion of the method; after detecting true positives, it is possible to target and record electrophysiologically from the presynaptic neurons and characterize them anatomically and physiologically. Input maps from a given presynaptic cell could then be obtained, so this method could be used sequentially to optically trace circuits.

Two-photon beam multiplexing could also be used to photorelease other neuroactive compounds with single-cell precision. It could be combined with the use of channelrhodopsins[27,28] or other genetically encoded probes, to extend the method for *in vivo* applications while still preserving single-cell resolution.

As this technique can be combined with two-photon calcium imaging, it can be used as an all-optical stimulation and recording method to quickly examine the connectivity of a circuit and explore the regimes in which different groups of neurons are activated by the stimulation of sets of neurons, as if the researcher were 'playing the piano' with the circuit. This experimental approach seems an ideal one to understand the role of individual neurons in biological circuits and also, potentially, to reverse-engineer and decipher their transfer function.

METHODS

Custom two-photon microscope. Our system is a modification of a previously described custom two-photon fluorescence and second harmonic generation microscope[17,29]. Briefly, the microscope (**Supplementary Fig. 1**) consists of a laser, an electro-optical modulator (Pockels cell), beam-shaping optics (telescope and spatial filter), DOE optics, a scanner, an upright microscope and a photomultiplier-based two-photon fluorescence and second harmonic generation detection system. Specifically, we used a tunable titanium:sapphire laser (Chameleon; Coherent), a model 350-160 Pockels cell driven by a model 275 linear amplifier (Conoptics), intermediate dielectric mirrors (BB1-E02; Thorlabs) and a diffractive optical element (fused silica, type SLH-505Xa-(0.23)-(780); Stocker Yale Canada Inc.). We assembled all other elements of the optical path from standard components (Thorlabs). The upright microscope (Olympus BX50WI) was equipped with water-immersion objectives (Olympus). We used a LUMPlanFI/IR 40×, 0.8 numerical aperture (NA) lens (IR2 coating) for targeting cells in DIC for patch-clamping, and high-resolution two-photon imaging and photostimulation of small number of neurons, but we used low-magnification objectives (UMPlanFI 20×, 0.5 NA; XLUMPlanFI 20×, 0.95 NA; and UMPlanFI 10×, 0.3 NA) for imaging and photostimulation of neuronal populations. A short-pass dichroic mirror (type 650DCSP; Chroma Technology) was placed inside the standard trinocular tube of the microscope. An IR-blocking filter (type BG39; Chroma Technology) was placed in front of the photomultiplier to filter out remaining infrared light scattered from the excitation path. As a detector, we used a cooled GaAs photomultiplier (model H7422P-40; Hamamatsu) with an additional amplifier (PE 5113; Signal Recovery AMETEK Advanced Measurement Technology). We used a fast mechanical shutter (LS6T2; driven by a VCM-D1; Vincent Associates) to protect the photomultiplier from overloading in simultaneous imaging-uncaging experiments. Photomultiplier signals were digitized by the Fluoview board in raster mode or by an external data acquisition board in vector mode (model PCI-6052E; National Instruments). An analog output of this board also modulated laser intensity through the Pockels cell, according to the command from our custom software. The same software controlled the position of the scan mirrors through direct calls of functions in the original library files (gbx.dll; FV200 Olympus Fluoview Basic)[17]. The custom software was created in LabView programming environment (National Instruments) and communicated with integrated software routines for computationally intensive procedures such as cell-contour detection or traveling-salesman path computation (Matlab; Mathworks). All software can be freely downloaded from http://www.twophoton.com/software.

Slice preparation and loading. We prepared coronal neocortical slices from postnatal days 12–15 (P12–15) C57/BL6 mice or somatostatin-GFP mice[30] (Jackson Laboratory) with a vibratome (VT1000S; Leica). We cut 300-μm-thick slices in ice-cold

oxygenated modified artificial cerebro-spinal fluid (ACSF) that included 1 mM $CaCl_2$ and 3 mM $MgSO_4$, in which NaCl was replaced by an equimolar concentration of sucrose (in mM): 27 $NaHCO_3$, 1.5 NaH_2PO_4, 222 sucrose, 2.6 KCl. We then placed the slices in oxygenated standard ACSF at 37 °C for 30 min. For AM dye–loading, we deposited the slices onto the bottom of a small Petri dish (35 × 10 mm) filled with 2 ml of ACSF, ventilated with 95% O_2–5% CO_2 and placed in a slide warmer at 37 °C (Fisher Scientific). An aliquot of 50 μg indo-1 AM or mag-indo-1 AM (Molecular Probes) was prepared in 10 μl DMSO and 2 μl of Pluronic F-127 (Molecular Probes). For combined loading we used 50 μg indo-1 AM and 2 μg mag-indo-1 AM. We then placed the dye aliquot into the Petri dish and incubated the slices in the dark at 35–37 °C for up to 60 min. For double-labeling with mag-indo-1 AM and sulforhodamine 101, we applied sulforhodamine 101 (20 μM) for the last 15 min. We kept the slices at room temperature (20–26 °C) for at least 30 min before transferring them to the recording chamber. In experiments, we used standard ACSF continuously aerated with 95% O_2–5% CO_2, containing (in mM): 123 NaCl, 3 KCl, 26 $NaHCO_2$, 1 NaH_2PO_2, 10 dextrose, 1 $CaCl_2$ and 3 $MgSO_2$ for mapping experiments and loading, or same composition except with 3 $CaCl_2$ and 1 $MgSO_2$.

Two-photon uncaging of glutamate. MNI-caged glutamate (2.5 mM; Tocris Cookson) was bath-applied, and a Lambda (Bioptechs) or Dynamax RP-1 (Rainin) peristaltic micropump was used to control bath perfusion and minimize total bath volume. We analyzed electrophysiological recordings (to detect EPSP-like events time-locked to uncaging laser pulses) with custom software written in Matlab. For effective uncaging with shorter laser pulses, we used up to 25 separate beamlets. The development of more powerful lasers could allow larger multiplexing of the beam.

Additional methods. Details of input mapping protocols, electrophysiological methods and histological methods are available in **Supplementary Methods**. All experiments were performed in agreement with US National Institutes of Health Guide for the Care and Use of Laboratory Animals and after approval from the local Institutional Animal Care and Use Committee.

Note: Supplementary information is available on the Nature Methods website.

ACKNOWLEDGMENTS

We thank E. Callaway for advice, A. Packer for online analysis, B. Nemet for help with optics, G. Ellis-Davies for initial samples of MNI-glutamate, D. Aronov for the convex hull algorithm, Y. Duanmu for histology, and L. Abbott, E. Schaffer and members of the laboratory for comments. Supported by the US National Eye Institute, the National Institute of Neurological Disorders and Stroke, the New York State Foundation for Science Technology and Innovation (NYSTAR) program and the Kavli Institute for Brain Studies. K.E.P. is a Patterson Trust postdoctoral fellow. We dedicate this study to the memory of Larry Katz, who pioneered and stimulated these experiments.

Published online at http://www.nature.com/naturemethods/
Reprints and permissions information is available online at http://npg.nature.com/reprintsandpermissions

1. Sterling, P. Retina. in *The Synaptic Organization of the Brain* (ed. G.M. Shepherd) 170–213 (Oxford University Press, Oxford, 1990).
2. Crick, F.H. Thinking about the brain. *Sci. Am.* **241**, 219–232 (1979).
3. Farber, I.C. & Grinvald, A. Identification of presynaptic neurons by laser photostimulation. *Science* **222**, 1025–1027 (1983).
4. Callaway, E.M. & Katz, L.C. Photostimulation using caged glutamate reveals functional circuitry in living brain slices. *Proc. Natl. Acad. Sci. USA* **90**, 7661–7665 (1993).
5. Dalva, M.B. & Katz, L.C. Rearrangements of synaptic connections in visual cortex revealed by laser photostimulation. *Science* **265**, 255–258 (1994).
6. Shepherd, G.M., Pologruto, T.A. & Svoboda, K. Circuit analysis of experience-dependent plasticity in the developing rat barrel cortex. *Neuron* **38**, 277–289 (2003).
7. Kotter, R., Schubert, D., Dyhrfjeld-Johnsen, J., Luhmann, H.J. & Staiger, J.F. Optical release of caged glutamate for stimulation of neurons in the *in vitro* slice preparation. *J. Biomed. Opt.* **10**, 11003 (2005).
8. Dodt, H.U., Schierloh, A., Eder, M. & Zieglgansberger, W. Circuitry of rat barrel cortex investigated by infrared-guided laser stimulation. *Neuroreport* **14**, 623–627 (2003).
9. Boucsein, C., Nawrot, M., Rotter, S., Aertsen, A. & Heck, D. Controlling synaptic input patterns *in vitro* by dynamic photo stimulation. *J. Neurophysiol.* **94**, 2948–2958 (2005).
10. Shoham, S., O'Connor, D.H., Sarkisov, D.V. & Wang, S.S. Rapid neurotransmitter uncaging in spatially defined patterns. *Nat. Methods* **2**, 837–843 (2005).
11. Denk, W., Strickler, J.H. & Webb, W.W. Two-photon laser scanning fluorescence microscopy. *Science* **248**, 73–76 (1990).
12. Canepari, M., Nelson, L., Papageorgiou, G., Corrie, J.E. & Ogden, D. Photochemical and pharmacological evaluation of 7-nitroindolinyl-and 4-methoxy-7-nitroindolinyl-amino acids as novel, fast caged neurotransmitters. *J. Neurosci. Methods* **112**, 29–42 (2001).
13. Ellis-Davies, G.C.R. Development and application of calcium cages. *Methods Enymol.* **360A**, 226–238 (2003).
14. Yuste, R. & MacLean, J. Loading populations neurons in slices with AM calcium indicators. in *Imaging Neurons: a Laboratory Manual* (eds. R. Yuste, F. Lanni & A. Konnerth) 351–355 (Cold Spring Harbor Press, Cold Spring Harbor, NY, 2005).
15. Nimmerjahn, A., Kirchhoff, F., Kerr, J.N. & Helmchen, F. Sulforhodamine 101 as a specific marker of astroglia in the neocortex *in vivo*. *Nat. Methods* **1**, 31–37 (2004).
16. Cossart, R., Aronov, D. & Yuste, R. Attractor dynamics of network UP states in neocortex. *Nature* **423**, 283–289 (2003).
17. Nikolenko, V., Nemet, B. & Yuste, R. A custom two-photon and second harmonic microscope. *Methods* **30**, 3–5 (2003).
18. Peterlin, Z.A., Kozloski, J., Mao, B., Tsiola, A. & Yuste, R. Optical probing of neuronal circuits with calcium indicators. *Proc. Natl. Acad. Sci. USA* **97**, 3619–3624 (2000).
19. Sacconi, L.F.E., Antolini, R., Taghizadeh, M.R., Choudhury, A. & Pavone, F.S. Multiphoton multifocal microscopy exploiting a diffractive optical element. *Opt. Lett.* **28**, 1918–1920 (2003).
20. Yoshimura, Y., Dantzker, J.L. & Callaway, E.M. Excitatory cortical neurons form fine-scale functional networks. *Nature* **433**, 868–873 (2005).
21. Le Be, J.V. & Markram, H. Spontaneous and evoked synaptic rewiring in the neonatal neocortex. *Proc. Natl. Acad. Sci. USA* **103**, 13214–13219 (2006).
22. Yuste, R. & Katz, L.C. Control of postsynaptic Ca^{2+} influx in developing neocortex by excitatory and inhibitory neurotransmitters. *Neuron* **6**, 333–344 (1991).
23. Kozloski, J., Hamzei-Sichani, F. & Yuste, R. Stereotyped position of local synaptic targets in neocortex. *Science* **293**, 868–872 (2001).
24. Wang, Y. *et al.* Anatomical, physiological and molecular properties of Martinotti cells in the somatosensory cortex of the juvenile rat. *J. Physiol. (Lond.)* **561**, 65–90 (2004).
25. Badea, T., Goldberg, J., Mao, B.Q. & Yuste, R. Calcium imaging of epileptiform events with single-cell resolution. *J. Neurobiol.* **48**, 215–227 (2001).
26. Trevelyan, A.J., Sussillo, D., Watson, B.O. & Yuste, R. Modular propagation of epileptiform activity: evidence for an inhibitory veto in neocortex. *J. Neurosci.* **26**, 12447–12455 (2006).
27. Boyden, E.S., Zhang, F., Bamberg, E., Nagel, G. & Deisseroth, K. Millisecond-timescale, genetically targeted optical control of neural activity. *Nat. Neurosci.* **8**, 1263–1268 (2005).
28. Zhang, F. *et al.* Multimodal fast optical interrogation of neural circuitry. *Nature* **446**, 633–639 (2007).
29. Majewska, A., Yiu, G. & Yuste, R. A custom-made two-photon microscope and deconvolution system. *Pflügers Arch.* **441**, 398–409 (2000).
30. Oliva, A.A., Jr., Jiang, M., Lam, T., Smith, K.L. & Swann, J.W. Novel hippocampal interneuronal subtypes identified using transgenic mice that express green fluorescent protein in GABAergic interneurons. *J. Neurosci.* **20**, 3354–3368 (2000).